Catalysis Science & Technology

Accepted Manuscript

ROYAL SOCIETY OF CHEMISTRY

www.rsc.org/catalysis

Journal Name

RSCPublishing

ARTICLE

Rational design of ethanol steam reforming catalyst based on analysis of Ni/La_2O_3 metal-support interactions

Cite this: DOI: 10.1039/xoxxoooooox

Received ooth January 2012,
Accepted ooth January 2012

DOI: 10.1039/xoxxoooooox

www.rsc.org/

Jyong-Yue Liu[a], Wei-Nien Su[b], John Rick[a], Sheng-Chiang Yang[a], Chun-Jern Pan[a], Jyh-Fu Lee[c], Jin-Ming Chen[c] and Bing-Joe Hwang[a,c,*],

Understanding the metal-support interactions between Ni and La_2O_3 has helped us design an improved catalyst for the ethanol steam reforming reaction (ESR). Information from *in situ* X-ray absorption spectra (XAS) and high-resolution transmission electron microscopy (HRTEM) has helped us to prepare a Ni-based catalyst, in which strong metal-support interactions (SMSI) maximize the hydrogen yield by suppressing undesired reaction pathways. It was found that the Ni, formed as nanoparticles, was well-dispersed both in and on the La_2O_3. The Ni/La_2O_3 catalyst, when compared to a Ni/SiO_2 catalyst, yielded twice as much H_2 (3.7 molH_2 mol^{-1}EtOH) at 395℃ by both inhibiting methanation ($CO + 3H_2 \rightarrow CH_4 + H_2O$) and promoting the water gas shift reaction ($CO + H_2O \rightarrow CO_2 + H_2$). It is expected that our enhanced understanding of Ni/La_2O_3 physical/chemical interactions will help us design new catalysts for various catalytic applications.

Introduction

With increasingly rapid industrialization the need to satisfy growing energy demands has been thrown into sharp focus[1]. Fossil fuels, due to cost and ease of extraction, are still the main global energy source; however, the ongoing consumption of fossil fuels is creating serious environmental problems. How to address these problems is an important unresolved issue.

Among the renewable energy technologies e.g. solar energy, wind power, marine energy etc.; hydrogen fuel cells that use hydrogen, sourced from hydrocarbons or ethanol, offer conversion efficiency and environmental benefits[2]. Of the means used to generate hydrogen, ethanol steam reforming[3-5] [(ESR) $C_2H_5OH + 3H_2O \rightarrow 6H_2 + 2CO_2$] is commonly preferred, due to its minimal environmental impact[6 7].

Transition metals such as Rh, Pt, Ru, Pd Ir, Co, Ni, Cu and Fe[8] show significant activity and selectivity for ESR, of these Rh shows a particularly impressive activity; however its high cost limits its more widespread application. Apart from the noble metals, Ni shows promise, due to its C-C and OH bond breaking activity[9]. However, Ni-base catalysts still face issues related to their high working temperature window (>500℃), sintering and coke deposition. Many authors have proposed strategies to prevent coke deposition and agglomeration on Ni based catalysts, e.g. Nichele *et al.*,[10] used CaO-doped Ni/ZrO_2 to improve coking resistance, while Carrero *et al.*,[11] used Cu-Ni, supported on high surface area SBA-15 a, to prevent sintering at high temperatures.

The pathways for hydrogen production in a generalized ESR scheme[9] are shown below:

Dehydrogenation: $C_2H_5OH \rightarrow C_2H_4O + H_2$

Acetaldehyde decomposition: $C_2H_4O \rightarrow CH_4 + CO$

Acetaldehyde steam reforming: $C_2H_4O + H_2O \rightarrow 3H_2 + 2CO$

In addition to the main reaction pathways, some important side-reactions may occur:

Water gas shift reaction (WGSR): $CO + H_2O \rightarrow CO_2 + H_2$

Methanation: $CO + 3H_2 \rightarrow CH_4 + H_2O$

Ni is a well-known methanation catalyst[12]: during low temperature ESR (<500℃), methanation may occur consuming large volumes of H_2 and CO. Generally, catalytic methanation on supported nickel catalysts is dependent on the active phase's particle or crystal size[13] and the interactions between the active metal and its support (SMSI)[14]. If this side reaction can be suppressed we can potentially maximize hydrogen yield, reduce energy loss, and minimize catalytic sintering.

Recently, SMSI have been widely discussed[15-17] and interpreted in terms of how electron transfer can lead to tailored catalytic properties[18]. The catalysts derived from ABO_3 perovskite have many features that encourage their use in the dry reforming of methane (DRM)[19, 20], the ESR[21, 22] and oxidative ethanol steam reforming (OESR)[23 24, 25]. $LaNiO_3$ is an easy reducible perovskite structure that was first used by de Lima *et al.*,[21] in a partially reduced form, to enhance ESR activity and stability. However, the current literature focus remains on how carbon formation can be inhibited, on the dispersed metal particles during ESR[26, 27]. At the time of writing, little experimental evidence has been offered to substantiate the existence of SMSI and how they affect reaction paths. To address this issue and explore the underlying catalytic mechanism we prepared two catalysts with supports shown to be inert towards

ESR: (i) Ni/La_2O_3 derived from perovskite, and (ii) Ni/SiO_2 prepared by a sol-gel method with a similar Ni loading/size.

Experimental

Catalyst preparation

$LaNiO_3$, was prepared using a co-precipitation method. Initially, 0.6M 100 mL solutions of both aqueous lanthanum nitrate hexahydrate (98 % ACROS) and nickel nitrate hexahydrate (99% ACROS) were mixed (1:1 molar ratio) and stirred while $NaOH_{aq}$ (3.2 M of 400 mL) was added dropwise (for 1 hr) to produce precipitation. The suspension was filtered and repeatedly washed with DI water, and the product dried at 110 ˚C overnight. Finally, the sample was calcined at 400 ˚C for 2 hr and then at 700 ˚C for 6 hr (ramp rate 5˚C/min). The catalyst derived from $LaNiO_3$ is denoted as Ni/La_2O_3. The sol gel method[28] was used to synthesize Ni/SiO_2. Nickel nitrate hexahydrate (0.01 mole, 99% ACROS) and citric acid (0.015 mole) were dissolved into 100 mL absolute ethanol and stirred at 60 ˚C for 4h. Then, a solution of deionized water and absolute ethanol (molar ratio, 3:1) was added. Tetraethyl orthosilicate (5.62g, TEOS) was added dropwise into the solution. After drying at 80 ˚C overnight, the precursor was calcined at 450 ˚C under air for 3h. All catalysts were reduced *in situ* in hydrogen at various temperatures. For the Ni/La_2O_3 catalyst, the reduction was performed at 550℃ for 1 hr (heating rate 7℃/min); while for Ni/SiO_2 the reduction was performed at 600℃ for 1hr. The Ni loading for both samples was 26.5wt%.

Characterization

Specimens were characterized using X-ray powder diffraction (XRD) with either a Bruker, D2 Phaser- X-ray powder diffraction spectrophotometer (in house), or by using the synchrotron light source (to record *in situ* XRD) at the Beam Line 01C (National Synchrotron Radiation Research Center (NSRRC), Hsinchu, Taiwan). The electron storage ring was operated at 1.5 GeV with a beam current of 100-200 mA. The XRD pattern was recorded using a wavelength of 0.5167 Å for limited angular regions at room temperature. The wavelength was changed to 1.5418 Å as the energy of $CuK_{\alpha 1}$. The crystallite size of the nickel was estimated using the Scherrer equation. *In situ* X-ray absorption spectra (XAS) were obtained using the Beamline 17C and 20A at the NSRRC as above. The electron storage ring was operated at 1.5 GeV with a beam current of 300 mA. Hard XAS were recorded at the Beamline 17C, with a double Si (111) crystal monochromator being used for energy selection. One collimating mirror and one refocusing mirror, both coated with Rh, were respectively located upstream and downstream of the monochromator. These two mirrors also served to reject high harmonics. The focused beam size at the sample position was 4 x 2 mm^2. Soft XAS, made in fluorescence mode for the oxygen K-edge, using an ultrahigh-vacuum (UHV) chamber with a base pressure of 1 x 10^{-10} Torr, were recorded at the Beamline 20A. A 6 m high energy spherical grating monochromator (6 m-HSGM) was used to perform the energy scan. High-resolution transmission electron microscopy (HRTEM) was conducted using a Philips Tecnai F30 FEI-TEM at an acceleration voltage of 200 kV. The powder samples for the HRTEM were prepared (in ethanol) by ultrasonic dispersion, prior to deposition and drying on carbon-coated copper grids. The reduction behaviour of the samples was measured by temperature programmed reduction (H_2-TPR), controlled by an AutoChem II. Samples (50 mg) were heated in 10% H_2 at a flow rate of 30 ml min^{-1}, with the temperature being increased from room temperature to 600 ˚C. Prior to the H_2 uptake experiment, all catalysts were reduced *in situ* in 10% H_2/N_2 at various temperatures (1 hr) and then cooled to room temperature using high purity N_2.

Catalytic activity measurement

The samples' catalytic activities with respect to the ESR reaction were evaluated at atmospheric pressure in a fixed-bed. Catalyst (50 mg) was placed in a quartz tubular reactor allowing activity to be evaluated using stepwise temperature changes from 325 to 500˚C (ramp rate 1℃/min) with 30 minutes waiting time for reaction equilibrium at each analysis reaction temperature with measurements taken for each 35℃ reaction temperature increase. A liquid reactant mixture of (H_2O/EtOH = 6) molar ratio was introduced at a flow rate of 0.005 mL/min and further eluted by He (15 mL/min). The weight hourly space velocity (WHSV = 1.74 h^{-1}) was defined as the ratio between the inlet feed (ethanol) mass flow rate and the mass of catalyst. It is to note that higher steam/ethanol ratio was meant for evaluation of catalyst but the condition is also associated with higher energy penalty. Prior to the reaction, samples were activated, by reduction with 10 % hydrogen (at a temperature determined by temperature programmed reduction (H_2-TPR) measurements) for 1 hour to ensure the nickel species (NiO or $LaNiO_3$) was reduced to metallic Ni. The gaseous products were characterized by gas chromatography (GC) on an Acme 6100 equipped with a pulsed discharge helium ionization detector (PDHID). Three factors were selected to evaluate the ESR reaction of the samples: (i) the conversion of ethanol [$X_{Ethanol}$(%)], (ii) the product distribution [P_i(%)] and (iii) the hydrogen yield (Y_{H2}) which was calculated by the mole ratios of $M_{Ethanol}$ and products (M_i), as defined by Equations (1) , (2) and (3), respectively:

$$X_{Ethanol}(\%) = \frac{M_{Ethanol,in} - M_{Ethanol,out}}{M_{Ethanol,in}} \times 100 \quad (1)$$

$$P_i(\%) = \frac{M_i}{M_{CH3CHO} + M_{H_2} + M_{CO} + M_{CO_2} + M_{CH_4}} \times 100 \quad (2)$$

$$Y_{H2}(\%) = \frac{M_{H_2}}{M_{Ethanol,in} - M_{Ethanol,out}} \times 100 \quad (3)$$

Results and discussion

H_2-TPR and Morphology analysis

Profiles (a) and (b) in Figure 1 represents H_2-TPR measurements of the $LaNiO_3$ (perovskite type), and the as-prepared Ni/SiO_2 samples, respectively. The $LaNiO_3$ shows three reduction peaks at 305˚C, 339˚C and 489˚C, with the first two slightly overlapping. By referring to the results of *in situ* XRD in Figure 2, the first reduction peak at 305˚C was identified as originating from the partial reduction of $LaNiO_3$, i.e. with the perovskite phase retained, the second reduction peak at 339˚C was identified as Ni metal, reduced from NiO, which indicates that not all Ni participates in the perovskite phase. Finally, the third peak at 489˚C is associated with the complete reduction of bulk perovskite. The as-prepared Ni/SiO_2 showed three main reduction peaks. The first two at 329 and 402˚C represent the reduction of NiO to Ni, while the broad reduction peak at 534˚C is associated with Ni release from the SiO_2 matrix.

The TEM image of $LaNiO_3$ perovskite (particle diameters ~ 50-100 nm) is shown in Figure 3(a). The Ni/La_2O_3 catalyst is shown in Figures 3(b), (c) and (d). Comparing Figure 3(a) $LaNiO_3$ and Figure

3(b) i.e. after pretreatment with 10 % H_2 at 550 ˚C for 1 hr, it is apparent that the perovskite phase is transformed – this observation is in good agreement with the *in situ* XRD (Figure 2). Notable are the well-dispersed Ni nanoparticles (NPs) on the La_2O_3 support (average diameter 5.9 nm, see TEM results; and XRD Figure S1). Interestingly, Figure 3(c) and the enlarged section of Figure 3(d) show one Ni NP with a clear Ni (111) lattice on La_2O_3 surrounded by the lanthanum oxide support. This indicates that Ni NPs can be partially embedded into the La_2O_3 support after reduction. For the Ni/SiO_2 catalyst shown in Figure 4, the Ni NPs are well dispersed (average diameter of 6 nm, see TEM results; and XRD Figure S2). From the above results, the Ni/La_2O_3 and Ni/SiO_2 catalysts have similar Ni particle sizes.

Analysis of strong interaction between the Ni and La_2O_3

In situ XAS was used to study the electronic structures of the Ni/La_2O_3 and Ni/SiO_2 catalysts. Figure 5 shows the Ni K-edge XANES of the Ni/La_2O_3 and Ni/SiO_2 catalysts (metallic Ni foil is also included as a reference). The dominant XANES peak (white line, denoted as WL) at the Ni K-edge is an absorption threshold resonance, which is assigned to the allowed orbital transition from 1s to 4p[29]. As shown in this figure, the Ni/La_2O_3, Ni/SiO_2 and metallic Ni foil had the same resonance, thereby indicating that the oxidation state of Ni in the Ni/La_2O_3 and Ni/SiO_2 catalysts was that of metallic Ni. However, a white line of slightly higher intensity was obtained for Ni/La_2O_3, suggesting that the Ni atoms' orbital electron density was modified by interaction between the Ni NPs and the La_2O_3 support[30]. The interaction between the Ni NPs and the La_2O_3 support was examined using O K-edge XAS on Ni/La_2O_3 and Ni/SiO_2, as shown in Figures 6 and 7 respectively. To facilitate comparison, La_2O_3, SiO_2 and $LaNiO_3$ samples are also included as references. The spectra reveal excitations from the O 1s orbital to unoccupied states [31]. The O K-edge spectrum of the Ni/La_2O_3 catalyst in Figure 6 (a) has two major excitation peaks: O 1s to Ni 3d – O 2p from 530 to 531.7 eV and O 1s to La 5d – O 2p from 533 to 537 eV. The small shoulder from 530 to 531.7 eV is due to the transitions of the O 1s electron to the antibonding O 2p state hybridized with the 3d metal states[32]. In contrast to Ni/La_2O_3 catalyst, there is no peak between 530 and 531.7 eV for Ni/SiO_2, see Figure 7(a) which indicates that there is no strong interaction between Ni and the SiO_2 support. This result can be explained by the chemical environment of the Ni NPs in Ni/La_2O_3 in which most Ni NPs formed by reduction migrate from the lattice to the surface[33], while others become partially embedded in the lanthanum oxide, producing multiple interfaces between the Ni and its support.

Evaluation of catalytic activity

Figure 8 shows ESR reaction conversion profiles as a function of reaction temperature (℃) from 325 to 500℃. At 325℃ the Ni/SiO_2 catalyst shows a maximal conversion of ethanol (100 %), whereas the Ni/La_2O_3 catalyst showed only 32% conversion; however, as the reaction temperature increased from 325 to 395℃, the conversion approached 100 %. Generally, ESR depends on the catalyst's 'active surface area' which may be the case with Ni/La_2O_3 and Ni/SiO_2, as the Ni NP sizes were similar [see, XRD (Figures S1 and S2) and [TEM (Figures 3 and 4)]. H_2 uptake data were obtained to determine the active areas, see Table S1. The H_2 uptakes for Ni/SiO_2 and Ni/La_2O_3 were 552.8 and 54.4μmole/g respectively; indicating that the main effect of SMSI is the suppression of H_2 adsorption[34] or metallic Ni partial embedding into the support to reduce the exposed Ni surface area .

Figure 9 shows ESR product distribution profiles, as a function of reaction temperature (℃), from 325 to 500℃, for Ni/SiO_2 and Ni/La_2O_3. For the Ni/SiO_2 catalyst at 325℃, H_2 (46.6%), CO (18.9%) and CH_4 (25.3%) were the main gaseous products, with a slight amount of CO_2 (9.2%). With the reaction temperature raised to 360℃, in addition to the main gaseous products H_2 (50.14%) and CH_4 (26.37%), the concentration of CO decreased to 0.34%, while the concentration CO_2 increased to 23.14%. The CO concentration remained low for temperatures between 395-465℃. At relatively high CH_4 concentrations our results agree with the existing catalytic Ni methanation literature[35]. The Ni/La_2O_3 catalyst was tested for comparison. At 325℃, H_2 (62.2%), CH_3CHO (20.2%), CO_2 (8.2%) and CH_4 (6.1%) were the main gaseous products with a slight amount of CO (3.3%). At 395℃, the concentration of CH_4 was ~8.3% with the CO being only ~1.6%. Within a reaction temperature window between 360 and 500℃, the Ni/La_2O_3 catalyst gave the greatest H_2 yield [(3.7 molH_2 mol^{-1}EtOH) at 395℃], with lower concentrations of methane, but higher CO.

The Ni/SiO_2 catalyst, having the largest surface area, gave the highest hydrogen yield below 360℃ (1.64 molH_2 mol^{-1}EtOH), c.f. Ni/La_2O_3 (0.51 molH_2 mol^{-1}EtOH). However, within the reaction temperature set between 360 and 500℃, the situation was reversed with the Ni/La_2O_3catalyst giving a greater H_2 yield. This may be explained as follows. After the dehydrogenation of ethanol, the acetaldehyde generated can undergo two competing reaction paths[36], (i) decomposition into CH_4 and CO ($CH_3CHO \rightarrow CO + CH_4$), or (ii) acetaldehyde steam reforming ($CH_3CHO + H_2O \rightarrow 2CO + 3H_2$). From either of these reaction paths, the water gas shift reaction (WGSR) can take place ($CO + H_2O \rightarrow CO_2 + H_2$)[37]. In contrast to Ni/La_2O_3, the Ni/SiO_2 catalyst produces less CO (0.3%) and more CH_4 (23.01%) at 395℃, implying that the Ni/SiO_2 catalyst also promotes methanation, producing methane and water by consuming CO and H_2.

In order to confirm this hypothesis, mixed gases comprising CO (29.5 torr), H_2(295 torr) and H_2O (334 torr) were used as reactants (at 395℃) with the two catalysts, as seen in Figure S3. For Ni/SiO_2 [Figure S3 (a)], H_2 (89%) and CH_4 (8.2%) were the main gaseous products plus CO_2 (2.8%), with most CO being consumed by methanation. In contrast, the case with Ni/La_2O_3, the concentrations of H_2, CH_4, and CO_2 were 92%, 1.1% and ~6.9% respectively. With this catalyst, the CO produced was more likely go through the WGSR. In addition, the CH_4/CO species in the given ESR with Ni/La_2O_3 were significantly suppressed. The SMSI significantly affects the reaction pathways by promoting the water gas shift reaction. The water dissociation provides the required oxygen source to remove CH_4/CO and this could be attributed to the La_2O_3 support and the SMSI between Ni and the support, as discussed in literature,[38, 39] where the interaction significantly enhances the ability of the admetal to dissociate the O-H bond in the adsorbed water molecule to produce a high hydrogen yield (Y_{H2}).[38] At 395 ˚C, the Ni/La_2O_3 catalyst showed the highest hydrogen yield (3.7 $mol_{H2}mol^{-1}_{EtOH}$), which clearly indicated its high ESR activity at mild temperatures, especially when compared with Ni/SiO_2 catalyst. Table 1 gives a comparative summary of the various Ni-based catalysts for ESR[40-43]. Despite differences in the steam/ethanol ratio, the Ni/La_2O_3 catalyst shows the highest hydrogen yield. From the observations and experiments above, we conclude that SMSI plays an important role in catalysis. We have demonstrated that the interactions can be effectively used to suppress methanation while generating higher hydrogen yields, thus helping us to design a superior catalyst for ethanol steam reforming.

Morphology and TGA analysis for used catalysts

The carbon balance for ESR reaction on Ni/La_2O_3 catalyst is shown in Table S2. Carbon deposition has been frequently mentioned in the literature as a problem associated with Ni based catalysts. Whisker carbon[44] or carbon nanotubes result from adsorbed carbon atoms on Ni particles, this adsorbed carbon later diffuses and nucleates into a carbon fiber[45]. The comparative morphologies of used Ni/La_2O_3 and used Ni/SiO_2 catalysts after the ESR reaction at 395℃ for 14 hr are shown in Figure 10. The sizes of the nickel NPs was ~ 8.3 nm for used Ni/La_2O_3 and 13 nm for used Ni/SiO_2. In addition, most carbon fibers, or carbon nanotubes, grew from metallic nickel.

Fatsikostas *et al.*,[46] proposed that the La_2O_3 support can react with CO_2 to form a lanthanum oxy-carbonate species that react with surface carbon, thereby removing carbon deposits by the reaction $La_2O_2CO_3 + C\text{-}Ni \rightarrow La_2O_3 + 2CO + Ni$. Thus, the $La_2O_2CO_3$ species is believed to function as a scavenger able to clean the deposited carbon from the Ni surface. As shown in Figure S4, the used Ni/La_2O_3 indeed exhibits similar XRD patterns to $La_2O_2CO_3$. Additionally, SMSI also inhibits coke deposition in close proximity to metallic Ni; however, the accumulation of carbon deposits may move particulate Ni away from the support[47, 48].

Coke deposition for Ni/SiO_2 and Ni/La_2O_3 was quantified using TGA measurements, see Figure S5. The TGA of used Ni/SiO_2 [Figure S5(a)] exhibited a weight loss (D_1) at around 400-600℃ that was the oxidation of carbon filaments[49], while, in contrast, the used Ni/La_2O_3 showed distinct weight losses in various temperature ranges i.e. 200-400℃ (D_1), 400-600℃ (D_2), 620-656℃ (D_3) and 656-718℃ (D_4), References [22, 49] suggesting that the ranges (D_2 and D_3) were the oxidation of carbon filaments and graphitic carbon respectively, and D_4 was thought to result mainly from the lanthanum decomposition, i.e.: $La_2O_2CO_3 \rightarrow La_2O_3 + CO_2$[50]. In addition, the weight gain D_1 was the oxidation of the nickel to nickel oxide. Furthermore, the total wt% of carbon was estimated to be about 18.5% for Ni/La_2O_3 and 57.8% for Ni/SiO_2. In addition to the support as a scavenger to remove the coke deposition, the less carbon deposits on Ni/La_2O_3 catalyst could be also due to the less exposed Ni particles, which are the active sites for carbon deposition. Furthermore, SMSI not only favours the dissociation of O-H bond to improve catalytic activity but also makes the cleavage of C-O bonds more difficult to prevent coke deposition by inhibiting the Boudouard reaction ($2CO \rightarrow C + CO_2$) during the ESR[51-53]. Therefore, as seen the case of Ni/La_2O_3, the strong interaction not only inhibits the particles from growing during the reaction at high temperatures, but also contributes to the decreased amount of carbon deposition. This physical/chemical phenomenon is not found with Ni/SiO_2.

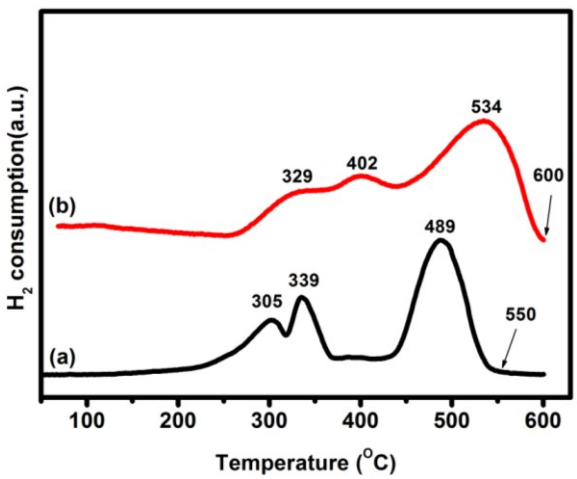

Fig. 1 H_2-TPR of (a) $LaNiO_3$, and (b) as prepared Ni/SiO_2 samples.

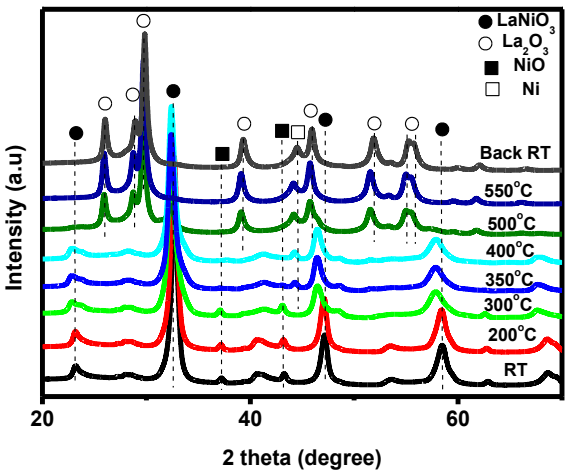

Fig. 2 *In situ* XRD patterns of $LaNiO_3$ sample with different reduction temperature.

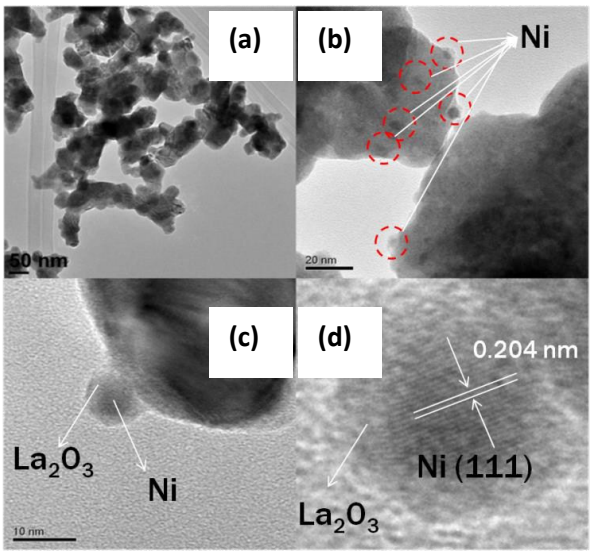

Fig. 3 TEM images of (a) $LaNiO_3$ sample, (b), (c) and (d) Ni/La_2O_3 catalyst (derived from $LaNiO_3$).

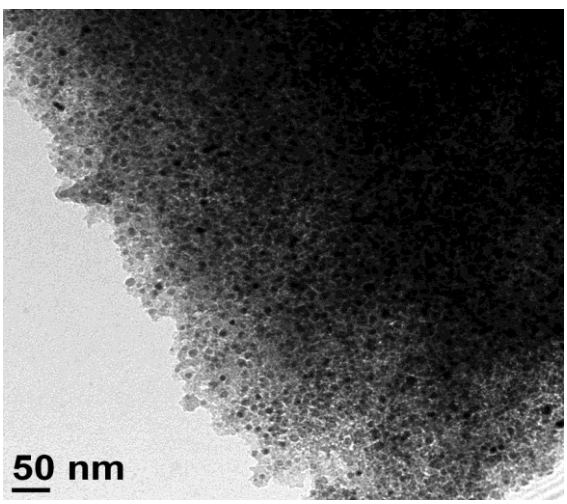

Fig. 4 TEM image of Ni/SiO_2 catalyst.

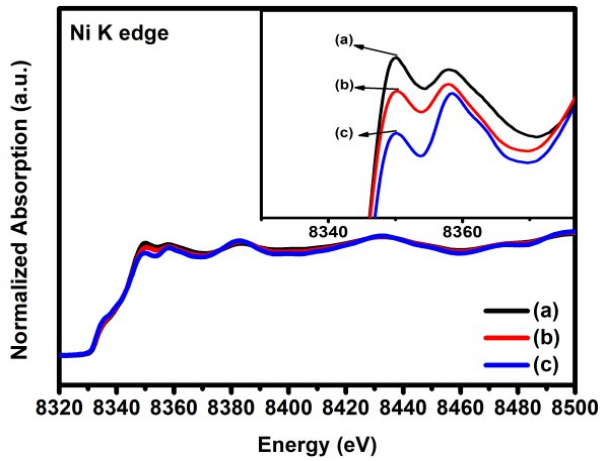

Fig. 5 XANES spectra of the Ni K-edge of (a) Ni/La_2O_3 catalyst, (b) Ni/SiO_2 catalyst and (c) metallic Ni foil sample

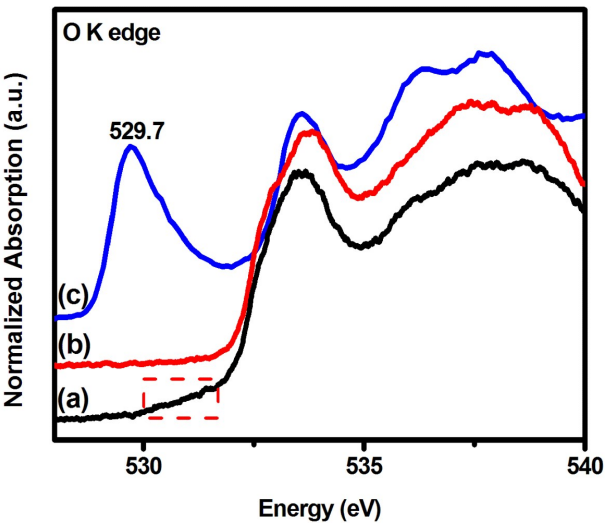

Fig. 6 XANES spectra of the O K-edge of (a) Ni/La_2O_3 catalyst, (b) La_2O_3 and (c) $LaNiO_3$ samples.

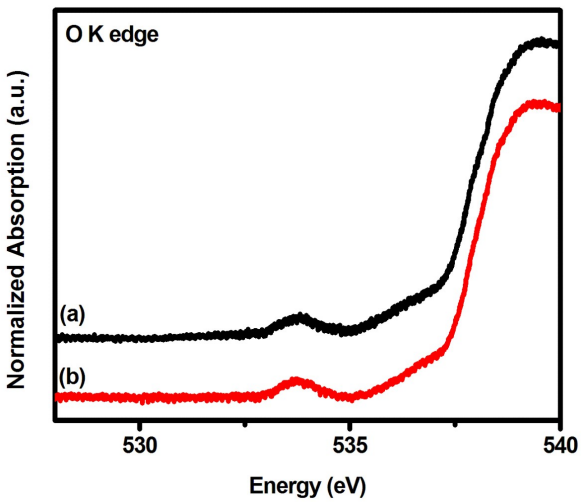

Fig.7 XANES spectra of the O K-edge of (a) Ni/SiO_2 catalyst and (b) SiO_2 sample.

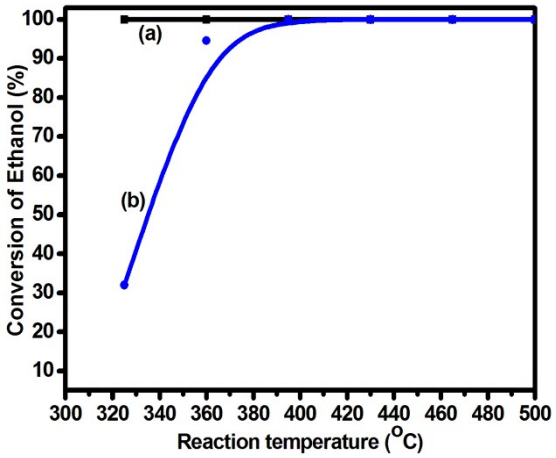

Fig. 8 ESR reaction of: ethanol conversion of (a) Ni/SiO_2 and (b) Ni/La_2O_3 catalysts with WHSV= 1.74 h^{-1} and $H_2O/EtOH$= 6.

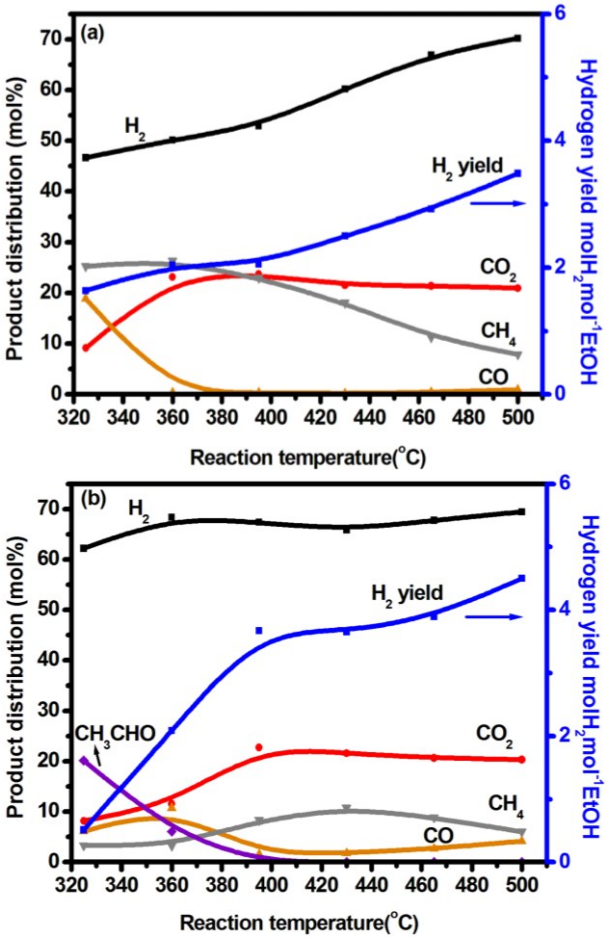

Fig. 9 ESR reaction of (a) Ni/SiO_2 and (b) Ni/La_2O_3 catalysts with WHSV= 1.74 h^{-1} and $H_2O/EtOH$= 6. The conversion of ethanol for all catalysts at the reaction temperature range between 395-500℃ were 100 %, and the temperature rate was 1℃/min, waiting 30 min for the reaction equilibrium at each analysis temperature that were taken every 35℃ increase in the reaction temperature.

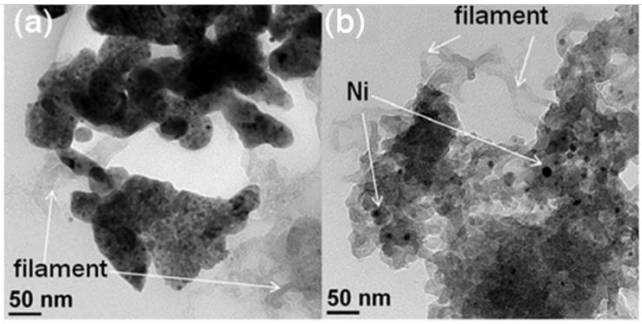

Fig.10 TEM images of used (a) Ni/La_2O_3, and (b) Ni/SiO_2 catalysts.

Table 1. Comparison of SRE performance of various Ni-based catalysts.

Catalysts	Reaction temp (°C)	H_2O/EtOH (molar ratio)	H_2 yield ($mol_{H2}mol^{-1}_{EtOH}$)	Ref.
Ni/La_2O_3	395	6	3.7	This study
Ni/SiO_2	395	6	1.8	This study
$CuNi/SiO_2$	400	3.7	1.1[a]	[40]
$CuNi/CeZrO_x$	400	8	2.4	[41]
CuNi/La20-SBA	600	3.7	3.8	[42]
$Ni_{0.5}Mg_{2.4}Cu_{0.1}$	450	3	3	[43]

[a] Derived from hydrogen selectivity, calculated according to the following equation:

$$S_{H2} = \frac{n_{H2}}{3(n_{Ethanol,in} - n_{Ethanol,out}) + (n_{H2O,in} - n_{H2O,out})} \times 100$$

Conclusions

In summary, using $LaNiO_3$ as the catalyst precursor; we observed, using X-ray absorption spectroscopy and HR-TEM analysis, nanosized Ni particles both supported on and embedded within the La_2O_3 support. SMSI was shown to inhibit methanation and enhance the stability of nanocatalyst, while promoting the WGSR during ESR. In comparison, coke formation on Ni/La_2O_3 was also significantly reduced. It was found that the Ni/La_2O_3 nanocatalyst showed a much higher hydrogen yield at 395℃, compared to the data reported in literature. Moreover, the work not only discusses the catalytic role of supports but also shows that the interaction between metal-support can significantly influence the reaction pathways. In addition to these effects, the SMSI prevented Ni NPs from agglomerating at high temperatures, while also suppressing coke deposition. We also demonstrate approaches of preparing nanocatalyst with desirable SMSI properties which can hold promise for the design and preparation of nanocatalysts for various heterogeneous reactions in the future.

Acknowledgements

The authors gratefully acknowledge the financial support from the Top Universities Project by the Ministry of Education (102H451401), National Science Council of Taiwan (NSC-99-2120-M-011-001), and National Taiwan University of Science and Technology (NTUST), as well as the facility supports from National Synchrotron Radiation Research Center (NSRRC).

Notes and references

[a] Department of Chemical Engineering, National Taiwan University of Science and Technology, Taipei 10617,Taiwan.
[b] Graduate Institute of Applied Science and Technology, National Taiwan University of Science and Technology, Taipei 10617, Taiwan.
[c] *National Synchrotron Radiation Research Center, Hsinchu 300, Taiwan*.

Electronic Supplementary Information (ESI) available: [details of any supplementary information available should be included here]. See DOI: 10.1039/b000000x/

1. S.-W. Liu, J.-Y. Liu, Y.-H. Liu, Y.-H. Huang, C.-T. Yeh and C.-B. Wang, *Catalysis Today*, 2011, 164, 246-250.
2. S. Li, M. Li, C. Zhang, S. Wang, X. Ma and J. Gong, *International Journal of Hydrogen Energy*, 2012, 37, 2940-2949.
3. S.-C. Yang, W.-N. Su, S. D. Lin, J. Rick and B.-J. Hwang, *Catalysis Science & Technology*, 2012, 2, 807-812.
4. M. Bilal and S. D. Jackson, *Catalysis Science & Technology*, 2012, 2, 2043-2051.
5. R. Dehghan-Niri, J. C. Walmsley, A. Holmen, P. A. Midgley, E. Rytter, A. H. Dam, A. B. Hungria, J. C. Hernandez-Garrido and D. Chen, *Catalysis Science & Technology*, 2012, 2, 2476-2484.
6. L. Liu, X. Ma and J. Li, *International Journal of Energy Research*, 2013, n/a-n/a.
7. S. J. Han, Y. Bang, J. Yoo, J. G. Seo and I. K. Song, *International Journal of Hydrogen Energy*, 2013, 38, 8285-8292.
8. J. L. Contreras, J. Salmones, J. A. Colín-Luna, L. Nuño, B. Quintana, I. Córdova, B. Zeifert, C. Tapia and G. A. Fuentes, *International Journal of Hydrogen Energy*, 2014, 39, 18835-18853.
9. M. Ni, D. Y. C. Leung and M. K. H. Leung, *International Journal of Hydrogen Energy*, 2007, 32, 3238-3247.
10. V. Nichele, M. Signoretto, F. Pinna, F. Menegazzo, I. Rossetti, G. Cruciani, G. Cerrato and A. Di Michele, *Applied Catalysis B: Environmental*, 2014, 150–151, 12-20.
11. A. Carrero, J. A. Calles and A. J. Vizcaíno, *Applied Catalysis A: General*, 2007, 327, 82-94.
12. R. D. Kelley and D. W. Goodman, *Surface Science*, 1982, 123, L743-L749.
13. J. M. G. Carballo, J. Yang, A. Holmen, S. García-Rodríguez, S. Rojas, M. Ojeda and J. L. G. Fierro, *Journal of Catalysis*, 2011, 284, 102-108.
14. J. Liu, *ChemCatChem*, 2011, 3, 934-948.
15. H. Wan, B. Wu, H. Xiang and Y. Li, *ACS Catalysis*, 2012, 2, 1877-1883.
16. J. Ohyama, A. Yamamoto, K. Teramura, T. Shishido and T. Tanaka, *ACS Catalysis*, 2011, 1, 187-192.
17. C. T. Campbell, *Nat Chem*, 2012, 4, 597-598.
18. B. H. Chen and J. M. White, *The Journal of Physical Chemistry*, 1982, 86, 3534-3541.
19. S. M. Lima, J. M. Assaf, M. A. Peña and J. L. G. Fierro, *Applied Catalysis A: General*, 2006, 311, 94-104.

20. G. S. Gallego, F. Mondragón, J. Barrault, J.-M. Tatibouët and C. Batiot-Dupeyrat, *Applied Catalysis A: General*, 2006, 311, 164-171.
21. S. M. de Lima, A. M. da Silva, L. O. O. da Costa, J. M. Assaf, G. Jacobs, B. H. Davis, L. V. Mattos and F. B. Noronha, *Applied Catalysis A: General*, 2010, 377, 181-190.
22. K.-H. Lin, C.-B. Wang and S.-H. Chien, *International Journal of Hydrogen Energy*, 2013, 38, 3226-3232.
23. H. Chen, H. Yu, F. Peng, G. Yang, H. Wang, J. Yang and Y. Tang, *Chemical Engineering Journal*, 2010, 160, 333-339.
24. S. M. Lima, J. M. Assaf, M. A. Peña and J. L. G. Fierro, *Applied Catalysis A: General*, 2006, 311, 94-104.
25. G. Valderrama, M. R. Goldwasser, C. U. D. Navarro, J. M. Tatibouët, J. Barrault, C. Batiot-Dupeyrat and F. Martínez, *Catalysis Today*, 2005, 107-108, 785-791.
26. D. L. Trimm, *Catalysis Today*, 1997, 37, 233-238.
27. J. R. Rostrup-Nielsen, *Journal of Catalysis*, 1984, 85, 31-43.
28. C. Wu and P. T. Williams, *Environmental Science & Technology*, 2010, 44, 5993-5998.
29. G. J. Colpas, M. J. Maroney, C. Bagyinka, M. Kumar, W. S. Willis, S. L. Suib, P. K. Mascharak and N. Baidya, *Inorganic Chemistry*, 1991, 30, 920-928.
30. A. K. Agegnehu, C.-J. Pan, J. Rick, J.-F. Lee, W.-N. Su and B.-J. Hwang, *Journal of Materials Chemistry*, 2012, 22, 13849-13854.
31. J. Suntivich, H. A. Gasteiger, N. Yabuuchi, H. Nakanishi, J. B. Goodenough and Y. Shao-Horn, *Nat Chem*, 2011, 3, 546-550.
32. D. Chen, J. Zhong, X. Wu, Z. Wu, N. Mironova-Ulmane, A. Kuzmin and A. Marcelli, *Spectrochimica Acta Part A: Molecular and Biomolecular Spectroscopy*, 2008, 70, 458-461.
33. K. Takehira, *Catalysis Surveys from Asia*, 2002, 6, 19-32.
34. H. Orita, S. Naito and K. Tamaru, *The Journal of Physical Chemistry*, 1985, 89, 3066-3069.
35. G. Zhou, L. Barrio, S. Agnoli, S. D. Senanayake, J. Evans, A. Kubacka, M. Estrella, J. C. Hanson, A. Martínez-Arias, M. Fernández-García and J. A. Rodriguez, *Angewandte Chemie International Edition*, 2010, 49, 9680-9684.
36. L.-C. Chen and S. D. Lin, *Applied Catalysis B: Environmental*, 2011, 106, 639-649.
37. V. Palma, F. Castaldo, P. Ciambelli and G. Iaquaniello, *Applied Catalysis B: Environmental*, 2014, 145, 73-84.
38. A. Bruix, J. A. Rodriguez, P. J. Ramírez, S. D. Senanayake, J. Evans, J. B. Park, D. Stacchiola, P. Liu, J. Hrbek and F. Illas, *Journal of the American Chemical Society*, 2012, 134, 8968-8974.
39. H. Z. Stephen D. Davidson, Junming Sun and Yong Wang *Dalton Trans.*, 2014, 43, 11782-11802.
40. A. J. Vizcaíno, A. Carrero and J. A. Calles, *International Journal of Hydrogen Energy*, 2007, 32, 1450-1461.
41. P. Biswas and D. Kunzru, *Catal Lett*, 2007, 118, 36-49.
42. J. A. Calles, A. Carrero and A. J. Vizcaíno, *Microporous and Mesoporous Materials*, 2009, 119, 200-207.
43. X.-P. Yu, W. Chu, N. Wang and F. Ma, *Catal Lett*, 2011, 141, 1228-1236.
44. J. R. Rostrup-Nielsen, J. Sehested and J. K. Nørskov, in *Advances in Catalysis*, Academic Press, 2002, vol. Volume 47, pp. 65-139.
45. J. Rass-Hansen, C. H. Christensen, J. Sehested, S. Helveg, J. R. Rostrup-Nielsen and S. Dahl, *Green Chemistry*, 2007, 9, 1016-1021.
46. A. N. Fatsikostas and X. E. Verykios, *Journal of Catalysis*, 2004, 225, 439-452.
47. J. Catherine, P. Matthieu and J. Vincent, *Nanotechnology*, 2012, 23, 142001.
48. R. T. K. Baker, M. A. Barber, P. S. Harris, F. S. Feates and R. J. Waite, *Journal of Catalysis*, 1972, 26, 51-62.
49. A. A. A. Da Silva, L. O. O. Da Costa, L. V. Mattos and F. B. Noronha, *Catalysis Today*, 2013, 213, 25-32.
50. A. N. Shirsat, M. Ali, K. N. G. Kaimal, S. R. Bharadwaj and D. Das, *Thermochimica Acta*, 2003, 399, 167-170.
51. J. Carrasco, D. López-Durán, Z. Liu, T. Duchoň, J. Evans, S. D. Senanayake, E. J. Crumlin, V. Matolín, J. A. Rodríguez and M. V. Ganduglia-Pirovano, *Angewandte Chemie International Edition*, 2015, 54, 3917-3921.
52. J. Carrasco, L. Barrio, P. Liu, J. A. Rodriguez and M. V. Ganduglia-Pirovano, *The Journal of Physical Chemistry C*, 2013, 117, 8241-8250.
53. S. Senanayake, J. Evans, S. Agnoli, L. Barrio, T.-L. Chen, J. Hrbek and J. Rodriguez, *Topics in Catalysis*, 2011, 54, 34-41.

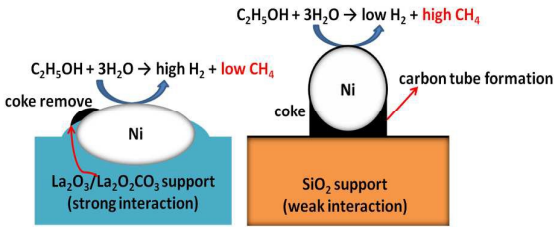

Ni/La_2O_3 nanocatalyst with strong interactions, compared to Ni/SiO_2, generated higher H_2 yield by suppressing the methanation reaction and coke deposition.